JOURNAL OF NATURAL REMEDIES
DOI: 10.18311/jnr/2025/51104
RESEARCH ARTICLE

Pharmacophore-guided Identification of Natural Compounds Targeting MAPK p38α for Inflammation-associated Asthma: Docking and Molecular Dynamics Insights

A. Varshini, R. Sanjana, Bhuvaneswari Sivaraman and Chagaleti Bharath Kumar*

Department of Pharmaceutical Chemistry, SRM College of Pharmacy, Faculty of Medicine and Health Sciences, SRM Institute of Science and Technology, Kattankulathur - 603203, Chengalpattu, Tamil Nadu, India; chagalek@srmist.edu.in

Abstract

Background: Asthma-associated inflammation is strongly linked to the activation of the p38α Mitogen-Activated Protein Kinase (MAPK) pathway, which mediates the production of pro-inflammatory cytokines and the recruitment of immune cells. Inhibition of p38α MAPK has therefore emerged as a promising therapeutic strategy for controlling airway inflammation. **Aim:** This study aimed to identify and characterize potential natural product-based inhibitors of p38α MAPK using an integrated computational approach combining pharmacophore modelling, virtual screening, molecular docking, ADMET prediction, and molecular Dynamics (MD) simulations. **Methods:** A ligand-based four-feature pharmacophore model was developed and validated (Sensitivity: 50.4%, Specificity: 80.2%, Accuracy: 79.9%) using known potent inhibitors Talmapimod, Doramapimod, Dilmapimod, Neflamapimod, AMG-548 and Losmapimod. The validated model was employed to screen 226,000 purchasable ZINC natural products, yielding 365 hits (MW ≤ 500 Da, RMSD ≤ 0.05 Å). Molecular docking studies using MOE identified top candidates based on binding affinity and key residue interactions. Physicochemical profiling and ADMET analyses were conducted to assess drug-likeness and safety, followed by 100 ns MD simulations to evaluate the dynamic stability of the best hit. **Results:** Docking results revealed that compounds SV1 (-8.99 kcal/mol; Tyr75, Glu71, Leu104) and SV2 (-8.94 kcal/mol; Met109) exhibited stronger binding affinities than the reference inhibitor Talmapimod (-8.50 kcal/mol). Both compounds satisfied Lipinski's Rule of Five and demonstrated favourable ADMET profiles. MD simulations confirmed the structural stability of SV1, with protein RMSD stabilizing at 3.2-4.2 Å, RMSF values mostly below 3.0 Å, a compact radius of gyration (5.2 Å), and consistent hydrogen bonding throughout the trajectory. **Conclusion:** The study identifies SV1 (ZINC38143592) as a potent, stable, and drug-like p38α MAPK inhibitor with potential for further development in managing asthma-related inflammation.

Major Finding: SV1 (ZINC38143592) demonstrated superior binding affinity, stability, and favourable pharmacokinetic properties, supporting its potential as a novel p38α MAPK inhibitor for asthma therapy.

Keywords: Asthma, Molecular Docking, Molecular Dynamics Simulation, p38α MAPK Inhibitors, Pharmacophore Modelling, Virtual Screening

Abbreviations: ADME – Absorption, Distribution, Metabolism, and Excretion; AKT – Protein Kinase B; BBB – Blood–Brain Barrier; CADD – Computer-Aided Drug Design; CYP – Cytochrome P450; DUD-E – Directory of Useful Decoys, Enhanced; ERK – Extracellular Signal-Regulated Kinase; GI – Gastrointestinal; HBA – Hydrogen Bond Acceptors; HBD – Hydrogen Bond Donors; IL – Interleukin; JNK – c-Jun N-terminal Kinase; LBDD – Ligand-Based Drug Design; MAPK – Mitogen-Activated Protein Kinase; MD – Molecular Dynamics; MolSA – Molecular Surface Area; MOE – Molecular Operating Environment; NF-κB – Nuclear Factor kappa-light-chain-enhancer of activated B cells; NPT – Constant Number, Pressure, and Temperature

*Author for correspondence

Article Received on: 14.08.2025 Revised on: 06.10.2025 Accepted on: 14.10.2025

ensemble; NVT – Constant Number, Volume, and Temperature ensemble; OPLS – Optimized Potentials for Liquid Simulations; PDB – Protein Data Bank; P-gp – P-glycoprotein; PRRs – Pattern Recognition Receptors; PSA – Polar Surface Area; rGyr – Radius of Gyration; RMSD – Root Mean Square Deviation; RMSF – Root Mean Square Fluctuation; RO5 – Rule of Five (Lipinski's); SASA – Solvent Accessible Surface Area; SBDD – Structure-Based Drug Design; TPSA – Topological Polar Surface Area; TNF-α – Tumour Necrosis Factor-alpha; WHO – World Health Organization.

1. Introduction

Asthma is a chronic inflammatory disease of the lungs that affects 262 million people worldwide. The disease involves inflammation and narrowing of the airways, making it difficult to breathe and potentially life-threatening[1]. The etiology of asthma is characterized by inflammation and hyper responsiveness of the airways. The process of inflammation in asthma is driven by various immune cells such as mast cells, eosinophils, dendritic cells and T-helper 2 (Th2) lymphocytes, which release cytokines production including interleukin IL-13, IL-4, and IL-5[2,3]. IL-5 promotes the recruitment and activation of eosinophils. At the same time, IL-13 and IL-4 are involved in the functional conversion of B cell antibody class to IgE production and the induction of goblet cell hyperplasia. These cytokines promote eosinophilic infiltration, goblet cell hyperplasia, mucus overproduction, and smooth muscle remodelling. As a result, the airways become narrowed, airflow is restricted, and characteristic asthma symptoms such as wheezing, coughing, and shortness of breath occur[4].

In asthma, environmental factors such as allergens, pollutants, and pathogens activate Pattern Recognition Receptors (PRRs) on airway epithelial cells and immune cells, leading to the stimulation of both PI3K-AKT-mTOR and MAPK signalling cascades. The pathophysiology of several diseases is significantly influenced by the Mitogen-Activated Protein Kinase (MAPK) cascade, including cancer, neurodegenerative disorders, and chronic inflammatory conditions. It mediates cellular responses to external stimuli such as stress, inflammation, and growth factors, thereby controlling cell proliferation, differentiation, survival, and the inflammatory mediator's production. The balance between MAPK activation (up regulation) and inhibition (down regulation) is essential for maintaining normal cellular functions[5]. The three main MAPK sub families are Extracellular signal-regulated Kinase (ERK), c-Jun N-terminal Kinase (JNK), and p38 MAPK. The p38α isoform, one of the four known isoforms (α, β, γ, and δ), is the most widely expressed and functionally dominant in bronchial epithelial cells and in immune cells such as mast cells, eosinophils, and macrophages. When activated by stress signals or allergens, p38α initiates the cytokines production like IL-1β, TNF-α, IL-6, and chemokines that attract other immune cells to the lungs. Because of its widespread presence and strong regulatory role in airway inflammation, p38α is considered the dominant isoform involved in the inflammatory processes in asthma[6].

Simultaneously, AKT-mTOR signalling acts as a crucial modulator of these MAPK-driven inflammatory processes. Activation of AKT promotes downstream mTORC1 signalling, which enhances protein translation, metabolic reprogramming, and cytokine biosynthesis. mTORC1 activation can also be induced by MAPK and, in turn, regulates MAPK activity, forming a reciprocal feedback loop that amplifies inflammatory signalling. This ensures coordinated regulation of MAPKs by primarily stabilizing and promoting transcription of cytokine mRNAs, whereas AKT-mTOR enhances their translation and secretion by increasing the cell's biosynthetic and metabolic readiness. Therefore, activation of AKT-mTOR not only supports MAPK-mediated inflammatory gene expression but also sustains the downstream production of pro-inflammatory mediators, establishing a feed-forward mechanism that contributes to chronic airway inflammation in asthma[7,8].

Potent drugs that target the MAPK p38 signalling pathway are Talmapimod, Doramapimod, Dilmapimod, Neflamapimod, AMG-548 and Losmapimod[9]. These drugs exhibit their action by lowering cytokine production, airway inflammation, and hyper responsiveness. Previous studies have emphasized the importance of heterocyclic scaffolds and bioactive small molecules in modulating inflammatory and metabolic pathways. For instance, 2-amino-4-arylthiazoles synthesized *via* green microwave-assisted methods have shown promising biological profiles and

synthetic efficiency under sustainable conditions[10]. Similarly, furan-based chalcones were reported to exert protective effects in diabetic zebrafish models by influencing PPAR-γ signalling and enhancing glucose uptake[11]. Such studies highlight the pharmacological relevance of heterocyclic derivatives in targeting pathways associated with AKT-mTOR-MAPK and related pro-inflammatory or metabolic mechanisms. Despite the efficacy of synthetic anti-inflammatory drugs, they frequently led to severe adverse effects such as gastrointestinal aggravation, cardiovascular hazards, immuno suppression, osteoporosis, adrenal suppression, and long-term metabolic disturbances[12,13]. Considering the limitations associated with synthetic anti-inflammatory agents targeting the p38 MAPK pathway, this study is intended to explore natural compounds as safer and more effective alternatives[14].

Natural compounds are biocompatible, possess fewer adverse effects and are frequently affordable. Numerous natural products exhibit multi-targeted anti-inflammatory effects, impacting major MAPK signalling pathways[15]. Several bioactive phytochemicals have been shown to decrease lung inflammation by targeting the MAPK pathway, including Fucosterol, Apigenin, Wagonin, Curcumin, and Resveratrol. Fucosterol from *Padina boryana* is a potent protector, activated via MAPK Pathways, that is induced by inflammatory conditions[16]. Apigenin lowers AKT, mTOR, JNK, and p38-MAPK, which lowers the Toll-like receptor-4-dependent activation of NF-κB[17]. Wogonin causes human breast cancer cells to produce reactive oxygen species and activate ERK and p38 MAPK signalling pathways to induce apoptosis[18]. Curcumin decreases IL-1 beta and matrix metalloproteinase-3, increases IL-10, and inhibits p38 mitogen-activated protein kinase activation in the mucosa of inflammatory bowel disease in adults and children[19]. Resveratrol prevents TNF-α-induced damage in human umbilical endothelial cells by encouraging Sirtuin-1-induced NF-KB and p38 MAPK Repression[20]. Based on the significance of phytochemicals, this study aims to investigate natural compounds from the library as potential modulators of the p38 MAPK pathway for the management of asthma-associated lung inflammation.

Computer-Aided Drug Design (CADD) is one of the important approaches in the drug discovery process. It provides an efficient way to find and optimise compounds in a cost-effective and time-efficient manner. CADD enables computational techniques to predict the interaction of small molecules with biological targets, thereby reducing extensive experimental procedures and accelerating the drug development process[21,22]. CADD involves two approaches: Ligand-Based Drug Design (LBDD) and Structure-Based Drug Design (SBDD). LBDD is employed when the 3D structure of the target is unknown, and the ligand is known. It is used to identify key pharmacophoric features, which are the spatial arrangement of functional groups required for biological activity[23]. Using these features, pharmacophore models are developed and applied for virtual screening to search natural product libraries for potential compounds. These potential hits are identified

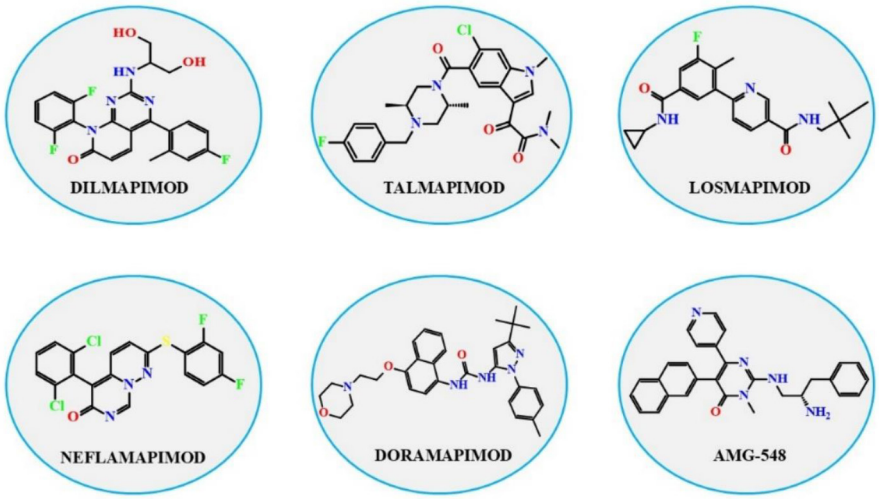


Figure 1. Inhibitors of p38α MAPK.

and are subjected to molecular docking, which predicts their binding affinity between the target and the ligand. The stability and conformational changes of the docked complexes are then assessed under Molecular Dynamics (MD) simulations. By integrating these computational techniques, the present study aims to identify and optimize natural compounds as potential MAPK inhibitors, supporting their development as promising therapeutic agents for the treatment of lung inflammatory disorders such as asthma.

2. Materials and Methods

2.1 Ligand Selection

A set of active inhibitors (Figure 1) targeting the p38α MAPK pathway such as Talmapimod, Doramapimod, Dilmapimod, Neflamapimod, AMG-548 and Losmapimod with reported IC_{50} values of 9 nM, 135 nM, 1 nM,29 nM,3 nM and 25nM respectively, were selected for pharmacophore model development based on a comprehensive literature review. These inhibitors target p38α MAPK, a key regulator in the release of pro inflammatory cytokines[24]. The chemical structures of these inhibitors were retrieved from PubChem and are energy-minimized utilizing the AMBER94x force field in MOE® 2022 software.

2.2 Generation of Pharmacophore Model

The energy-minimized inhibitors were aligned using the flexible alignment tool in MOE® 2022, with alignment parameters set to a failure limit of 20, an energy threshold of 50, and an iteration limit of 200[25]. To construct the pharmacophore features, the conformer exhibiting the highest alignment Score (S) indicating optimal structural overlap with minimal variability. The conformer with the highest alignment score was subsequently used to generate a common feature pharmacophore model *via* the pharmacophore query editor in MOE® 2022[26]. The consensus threshold was adjusted at an optimal tolerance of 1.2Å to identify the optimal pharmacophore features. MOE® utilises a built-in set of pharmacophoric features, such as: Aro|Hyd, Acc|Don, Acc2|Don2 and Acc. These features were utilized to generate a robust pharmacophore model capable of capturing key interactions essential for p38α MAPK inhibition.

2.3 Pharmacophore Validation

The set of actives and decoys for p38 alpha targeting was acquired from the DUD-E server[27]. These actives and decoys were used to validate the selected pharmacophore model. A set of parameters was utilised to assess the potential of the pharmacophore model. Sensitivity=TP/TP+FN; Accuracy=TP+TN/TP+FN+TN+FP and, Specificity=TN/TN+FP, where the terms True Positives (TPs), False Positives(FPs), False Negatives (FNs), and True Negatives (TNs), are utilised. These terms were calculated from the actives and decoys obtained using the query search module in MOE software.

2.4 Pharmacophore-based Virtual Screening

ZINC Pharmer, an online tool for potential hit identification that contains 37 billion chemical compounds, was used to perform pharmacophore-based virtual screening[28]. The validated pharmacophore model, developed in MOE® 2022, was uploaded to the ZINC database to search for structurally similar compounds. The ZINC purchasable natural products subset was utilized to identify drug-like compounds out of 230,000 compounds. Additional filters were applied to limit the molecular weight to ≤500. Hit compounds were evaluated based on their spatial fit with the pharmacophore features, using a Root Mean Square Deviation (RMSD) threshold of ≤0.05. The compounds were further retrieved and subsequently energy-minimized using the AMBER94x force field in MOE®.

2.5 Molecular Docking

Molecular docking is performed to evaluate the potential interactions between the active site of target protein and hitsidentified[29]. The target protein (PDB ID:4R3C) of p38α, an isoform of p38 MAP kinase co-crystallized with 3GF, GG5, classified under transferase, which is involved in the release of pro inflammatory cytokines, was obtained from the RCSB PDB[30]. The target protein consists of five chains with a resolution value of 2.06 Å. Molecular docking was executed in MOE® 2022. The protein structure was prepared by eliminating all water molecules, cofactors, and hetero atoms. In MOE, by using the Site Finder module, the binding site was predicted[31]. MOE dock module was then employed to dock the minimized structures onto the key amino acid residues of the p38α protein[32]. The docking poses were

evaluated using MOE's London dG scoring function, and the highest-ranked conformations were selected based on S-scores. Ligand-receptor interactions were visualized in both 2D and 3D representations.

2.6 Physicochemical Characteristics

Using SWISSADME software, the physicochemical property of the compounds was studied, with reference to the Lipinski rule to determine their oral bioavailability and drug-likeness[33]. According to this rule, a compound is likely to exhibit good oral bioavailability if it meets the following criteria: Octanol-water partition coefficient (log P) ≤ 5, Molecular Weight (MW) ≤ 500 Da, and Hydrogen Bond Acceptors (HBA) ≤ 10. These parameters reflect a compound's ability to cross biological membranes and interact with target proteins. Other descriptors like Topological Polar Surface Area (TPSA) and the number of rotatable bonds was also calculated as they influence solubility, polarity, molecular flexibility and drug pharmacokinetic behaviour.

2.7 ADMET Studies

The pharmacokinetic and toxicity profiles of the designed compounds were evaluated using *in silico* tools to predict their safety as drug candidates. Swiss ADME was employed to assess key ADME parameters, such as gastrointestinal absorption, P-glycoprotein interactions, blood-brain barrier permeability and cytochrome P450 enzyme inhibition[34,35]. These parameters help in understanding the behaviour of compounds that are absorbed, distributed, metabolized, and excreted within the body, which directly impacts their efficacy and safety. The ProTox-II tool was utilized to predict the toxicity profiles of the synthesized compounds, examining hepatotoxicity, carcinogenicity, immunotoxicity, mutagenicity, and cytotoxicity for safety evaluation[36,37]. Predicting toxicity through computational methods helps prioritize safer drug candidates, accelerating the development of effective and non-toxic drugs.

2.8 Molecular Dynamics

MD simulation was performed to study the changes in the solvent around the macromolecular complex using the Desmond V 5.9 program of the Schrodinger LLC package[38,39]. OPLS force field was utilized in enacting the dynamic simulations of the docked complex. The complex was placed in its centre inside an orthorhombic cubic cage with buffers and TIP3P water molecules to reproduce the dynamics. The average separation between each protein atom and the corners of box was nearly 10 Å. The presence of complex counter ions, such as Na^+ and Cl ion, was added to the calculation of the box volume in order to neutralize the system[40-42]. In order to keep to the minimal amount of heavy atoms on solute, the Desmond protocol has been used involving the use of OPLS-2005 force field parameters, and the Berendsen NVT is used to indicate a temperature of 10 K[43]. The simulation temperature was set to around 300 K, one atmosphere of pressure, and a relaxation time to 20 ps. In order to keep temperature and pressure constant, Nose Hoover thermostat and Martyna-Tobias-Klein barostat were used and the temperature was set to 300 K and pressure to 1 atm during simulation. There was an almost 100-ns span to the activation of the NPT ensemble. The paths of the generated frames were assessed and interpreted by means of simulation interaction diagrams.

3. Results and Discussion

3.1 Pharmacophore Model Generation

All the ligands were initially subjected to energy minimization, and a 3D pharmacophore model was built with MAPK inhibitors subjected to flexible alignment. Using the compute-pharmacophore query editor approach, the pharmacophore consensus was determined using the optimal flexible alignment conformation model. With a Fitness score (F) of -123.94, a Uniqueness score (U) of -63.35, and a Sum score (S) of -60.58, the best alignment results were obtained. The negative values of S indicate better alignment, a lower uniqueness score implies less strain, and lower fitness scores are indicative of lesser variability in the alignment. This alignment is the ideal arrangement of pharmacophore characteristics necessary for ligand binding and activity represented in the Figure 2. Initially, a threshold and tolerance of 100 % and 1.2 Å were used, which led to the identification of one feature F1:|Aro|Hyd|. In order to enhance the pharmacophore model accuracy, different thresholds were applied. Then, at threshold 83 %, 2 more features were suggested; F2|Acc| and F3:|Acc|. Finally, F4:|Acc2|Don2|was

identified at 67% of the threshold value. Figure 3 shows the pharmacophore model with four features, F1-F4. The best pharmacophore model was shown by four proposed features with a 100 % to 60% threshold value. Table 1 represents the four proposed features at a 1.2 Å tolerance. The best pharmacophore model is represented by Feature 1: |Aro|Hyd|;| Feature 2: |Acc|; Feature 3: |Acc|; Feature 4: |Acc2|Don2|.

3.2 Pharmacophore Validation

Pharmacophore model validation was performed using a dataset of 460 known active compounds and 36,428 decoys sourced from the DUDE (Database of Useful Decoys) server. The pharmacophore features were validated using query search module of MOE that predict the active and inactive compounds from the actives and decoys. The model yielded 182 true positives, 29,234 true negatives, 179 false negatives, and 7194 false positives. From these values, the model achieved a sensitivity of 50.4 %, indicating it successfully detected less than half of the actual active compounds. The specificity was 80.2%, reflecting a strong ability to correctly reject inactive compounds. The overall accuracy was 79.9%, indicating that the model was highly effective in distinguishing actives from inactives in the dataset.

Table 1. Features of the best pharmacophore model of MAPK p38α inhibitors

Code	Score %	Features	Radius Å
F1	100	Aro|Hyd	1.10
F2	83	Acc	0.91
F3	83	Acc	0.96
F4	67	Acc2|Don2	1.02

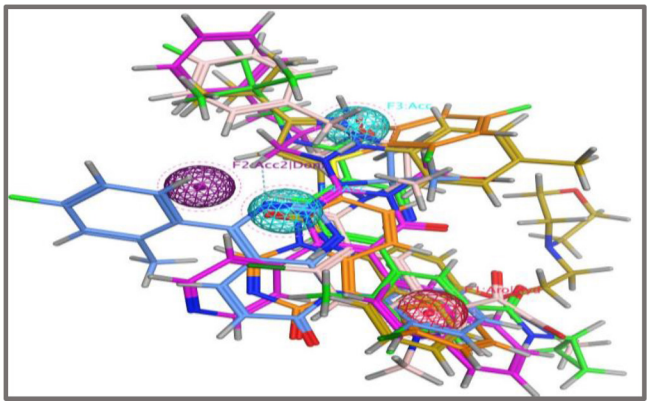


Figure 2. Best alignment model of the MAPK p38α inhibitors along with the pharmacophore features.

3.3 Pharmacophore Based Virtual Screening

Pharmacophore-based virtual screening was conducted utilizing the purchasable natural compounds subset of the ZINC database to identify potential hits possessing drug-like characteristics from the validated pharmacophore model. A molecular weight of fewer than 500 Daltons and an RMSD threshold of 0.05 Å were applied. Out of approximately 226,000 purchasable natural compounds available in the ZINC database, the virtual screening process resulted in 365 hit compounds that have matched both structural and pharmacophoric features. These selected natural molecules are further employed in *in silico* docking, pharmacokinetic profiling, and molecular dynamics.

3.4 Molecular Docking

Molecular docking was used to assess the binding interactions of 365 possible hits within the p38α active site**.** Table 2 displays the docking results of top ten screened compounds (SV1-SV10) were evaluated based on their binding affinity and amino acid interactions with the p38α MAPK protein, using Talmapimod as a standard. Molecular docking revealed docking scores ranging from -8.99 to -8.39 kcal/mol. Among the top ten compounds (SV1-SV10), SV1 (ZINC 38143592) and SV2 (ZINC04200785), exhibited the strongest affinity for binding of -8.99 kcal/mol, forming interactions with Tyr 75, Glu 71and Leu104 and 8.94kcal/mol with Met 109, respectively. Compared to Talmapimod which showed interaction with Pro 351, Lys 79, Lys 185 at a docking score of -8.50 kcal/mol. The Top 2

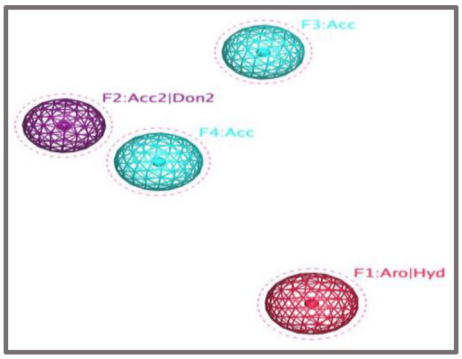


Figure 3. Pharmacophore model with features - F1: |Aro|Hyd|; F2: |Acc|; F3: |Acc|; F4: |Acc2|Don2|.

and standard compound interaction in 2D and 3D are provided in Figure 4. Whereas, SV3 (ZINC12885444) also showed a strong binding affinity of -8.82, forming interactions with Lys 53 and Met 109, enhancing stability. SV4 (ZINC04221871) showed a docking score of -8.59 and formed interactions with Leu 104, Asp 166, and Lys 53 of p38α MAPK.SV5 (ZINC 04221885), SV6 (ZINC 22061345) and SV7 (ZINC04221866) each established four key interactions with residues Asp 112, Lys 53, Met 109, Asp 168 and His 107 with binding affinities -8.54,-8.48 and -8.43Kcal/mol suggesting enhanced binding stability despite slightly lower docking energies. Compounds SV8, SV9, and SV10 exhibited comparable binding energies around -8.40, targeting residues like Lys 53, Met 109, and Ser 154. The frequent involvement of these residues across multiple ligands displays their importance as conserved binding elements within the protein's active site. Based on the overall docking studies, SV1 (ZINC 38143592) and SV2 (ZINC 04200785), with binding energy of -8.99 and -8.94 kcal/mol with favourable interaction profiles were considered promising leads for further optimization as potential p38 inhibitors.

3.5 Physicochemical Properties

The physicochemical characteristics of the top 10 docked compounds (SV1-SV10) are provided in Table 3, which were predicted using Swiss ADME. These properties show drug-like characteristics, indicating their potential as orally bio available therapeutic drugs. The compounds exhibit favourable lipophilicity profiles with log P values ranging from 1.15 (SV10) to 2.51 (SV6), all these compounds fall within the desirable range of 1-3 for oral bioavailability, indicating balanced hydrophilic-lipophilic characteristics necessary for membrane permeability and cellular uptake. All compounds' molecular weights remain below the 500 Daltons (472.49-498.56 Daltons), which satisfy Lipinski's rule of five[36]. The Topological Polar Surface Area (TPSA) values vary significantly from 161.29 Å² (SV8) to 210.45 Å² (SV9). Compounds like SV8 with lower TPSA values closer to the preferred <140 Å² may exhibit enhanced membrane permeability and high oral absorption compared to compounds like SV9 with higher TPSA values that may produce permeability challenges. Hydrogen bond acceptors range from 5 (SV8) to 11 (SV1) and donors from 3 (SV3) to 8 (SV5, SV10), where compounds with fewer hydrogen bond like SV8 are likely to give better permeability. The molecular flexibility, indicated by rotatable bonds in the range 3-12, shows compounds like SV6 and SV8 with minimal flexibility (3 bonds) producing enhanced target selectivity, while highly flexible compounds like SV3 and SV10 (12 bonds) may provide improved bioavailability but could lack in binding specificity. Compared to other docked compounds, compounds SV1 and SV2 appeared as the most potent compounds due to their optimal combination of appropriate log P values, lower TPSA, and reduced hydrogen bonding complexity, having high oral bioavailability and membrane permeation characteristics.

Table 2. Binding affinity of top ten compounds SV1-SV10 and standard (Talmapimod)

Compound Code	Docking Score Kcal/mol	Number of Interactions	Amino Acid Interaction
SV1	-8.99	3	Tyr 75; Glu 71(H-bonds); Leu 104(Hydrophobic)
SV2	-8.94	1	Met 109 (Hydrophobic)
SV3	-8.82	2	Lys 53 (H-bond); Met 109 (Hydrophobic)
SV4	-8.59	3	Leu104 (Hydrophobic); Asp 168; Lys 53 (H-bonds)
SV5	-8.54	4	Asp 112; Met 109; Lys53; Asp 168 (H-bonds)
SV6	-8.48	4	Ile 84; Lys 53; Asp 168; Asp 112 (H-bonds)
SV7	-8.43	4	Asp 112; Lys 53; Leu 108; (H-bonds) His 107 (Hydrophobic)
SV8	-8.40	2	Asp 168; Lys 53 (H -bonds)
SV9	-8.40	2	Met 109 (Hydrophobic); Asp 168 (H-bond)
SV10	-8.39	2	Asp168 (H-bond); Ser154 (Hydrophobic)
Standard (Talmapimod)	-8.50	3	Pro 351; Lys 79; Lys 185 (H-bonds)

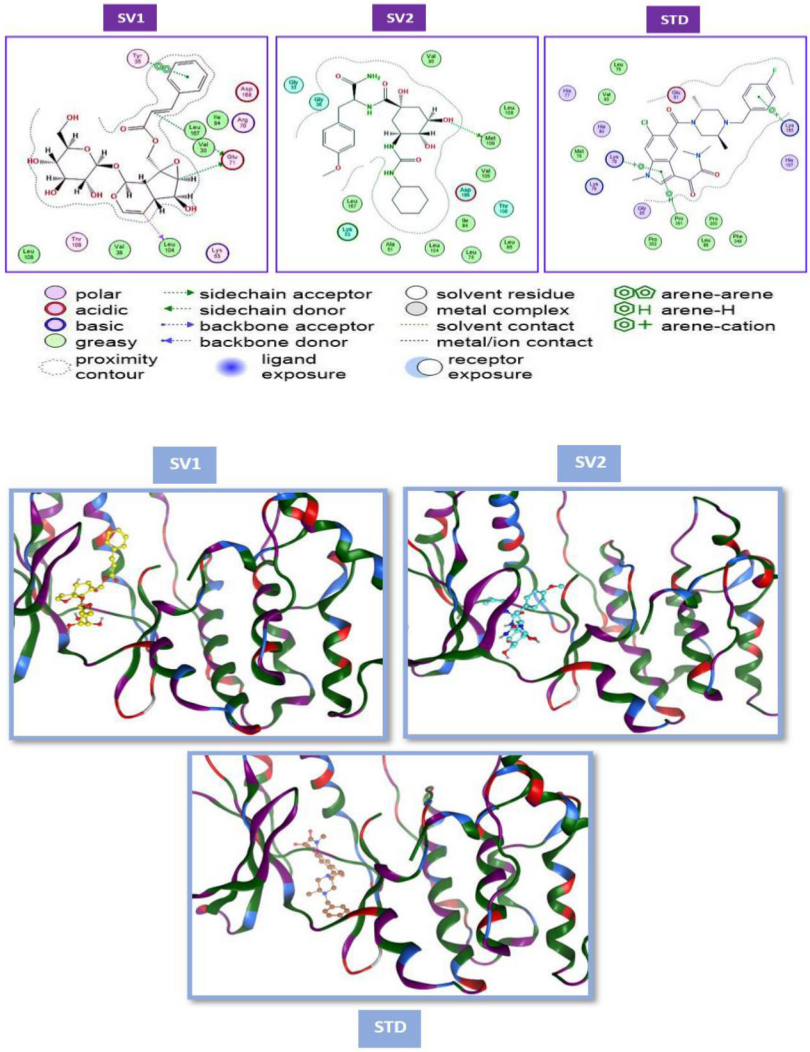


Figure 4. 2D and 3D representation of the top two compounds and the standard (Talmapimod).

Table 3. Physicochemical properties of top ten compounds SV1-SV10 and standard (Talmapimod)

Compound Code	Log P	TPSA (Å^2)	MW (Daltons)	HBA	HBD	No. of Rotatable Bonds
SV 1	1.84	167.67	492.47	11	5	8
SV2	2.21	183.24	492.57	7	7	11
SV3	2.07	168.35	480.49	6	3	12
SV4	1.75	184.10	472.49	8	6	10
SV5	1.25	194.24	490.48	8	8	10
SV6	2.51	178.23	498.50	9	5	3
SV7	1.44	199.45	491.56	7	6	11
SV8	2.17	161.29	484.55	5	6	3
SV9	2.37	210.45	477.53	7	7	10
SV10	1.15	198.82	481.56	7	8	12
Standard	4.17	65.86	513.00	5	7	0

3.6 ADME

The ADME (Absorption, Distribution, Metabolism, and Excretion) properties of the top ten compounds (SV1-SV10), are summarised in Table 4 using Swiss ADME, indicates important pharmacokinetic features relevant for oral drug development[37]. None of the compounds are predicted to be permeant to the Blood Brain Barrier (BBB), indicating less adverse effects on the central nervous system, favourable for peripheral drug targets. All compounds exhibited **low gastrointestinal absorption,** so that prodrug or formulation modification could enhance their oral bioavailability. Most of the compounds (except SV4, SV5, and SV10) are substrates for P-glycoprotein (P-gp), a transporter associated with reduced bioavailability as it promotes drug efflux from cells; this could be rectified by altering formulation strategies. The cytochrome P450 inhibition property shows that, except SV3 (which inhibits CYP3A4), all compounds are non-inhibitors for key CYP enzymes (CYP1A2, CYP2C19, CYP2C9, CYP2D6, CYP3A4), which have a desirable property that reduces the risk of drug-drug interactions and metabolic complications. The log Kp values (skin permeation) range from -8.02 to -9.98cm/s, indicating low trans dermal absorption. From these findings, SV1 and SV2 are optimum candidates due to their balanced ADME properties, including drug metabolism and distribution parameters.

3.7 Toxicity Profile

Toxicity prediction for compounds SV1 to SV10 was evaluated by five key toxicity parameters they are carcinogenicity, hepatotoxicity, mutagenicity, cytotoxicity, and immunotoxicity are summarised in Table 5. The majority of the compounds exhibited non-toxic (inactive). In hepatotoxicity, all compounds were predicted as inactive, with probabilities ranging from 0.61 to 0.84, indicating a less risk of liver damage **and** cancer. In carcinogenicity, each compound showed inactive results, with probability values between 0.59 and 0.77. This inactivity on the series of compounds suggests that they are unlikely to pose carcinogenic risks. Regarding mutagenicity, most compounds were predicted as inactive. SV2, SV5, SV8, SV9, and SV10 showed high probabilities (0.71-0.80), indicating low potential for mutagenic effects. These results further support the genetic safety of the designed compounds. In immunotoxicity, six of the ten test compounds (SV2, SV3, SV5, SV7, SV9, and SV10) were predicted as inactive. SV3 and SV9 had particularly high inactive probability scores (0.98 and 0.97, respectively), indicating their strong immunological safety. For cytotoxicity, all compounds were predicted as inactive, with probability values ranging from 0.62 to 0.72 **indicating** low cell toxicity. Overall, the compounds SV1 to SV10 exhibit promising safety profiles *in silico*, with strong inactive toxicity predictions across all categories. These findings

Table 4. ADME properties of the top ten compounds SV1-SV10 and standard (Talmopimod)

Compound Code	GI Absorption	BBB Permeant	P-GP Substrate	CYP1A2 Inhibitor	CYP2C19 Inhibitor	CYP2C9 Inhibitor	CYP2D6 Inhibitor	CYP3A4 Inhibitor	LOG KP (Skin Permeation)[cm/s]
SV 1	L	N	Y	N	N	N	N	N	-9.70
SV2	L	N	Y	N	N	N	N	N	-9.36
SV3	L	N	Y	N	N	N	N	Y	-8.36
SV4	L	N	N	N	N	N	N	N	-9.98
SV5	L	N	N	N	N	N	N	N	-9.69
SV6	L	N	Y	N	N	N	N	N	-8.02
SV7	L	N	Y	N	N	N	N	N	-9.59
SV8	L	N	Y	N	N	N	N	N	-8.54
SV9	L	N	Y	N	N	N	N	N	-9.73
SV10	L	N	N	N	N	N	N	N	-9.75
Standard	H	Y	N	N	Y	Y	Y	Y	-6.80

L- Low; H-High; N-No; Y-Yes

Table 5. Toxicity results of the top ten compounds SV1-SV10 and standard (Talmopimod)

Compound Code	Hepatoxicity		Carcinotoxicity		Mutagenicity		Immunotoxicity		Cytotoxicity	
	Toxicity	Prob	Toxicity	Prob	Toxicity	Prob	Toxicity	Prob	Toxicity	Prob
SV1	I	0.83	I	0.77	I	0.54	A	0.98	I	0.66
SV2	I	0.75	I	0.72	I	0.78	I	0.66	I	0.69
SV3	I	0.84	I	0.59	I	0.62	I	0.98	I	0.72
SV4	I	0.71	I	0.72	I	0.69	A	0.92	I	0.64
SV5	I	0.61	I	0.63	I	0.74	A	0.60	I	0.69
SV6	I	0.83	I	0.74	A	0.90	A	0.99	I	0.69
SV7	I	0.70	I	0.75	I	0.66	I	0.86	I	0.62
SV8	I	0.84	I	0.66	I	0.80	A	0.56	I	0.68
SV9	I	0.68	I	0.74	I	0.71	I	0.97	I	0.65
SV10	I	0.70	I	0.77	I	0.77	I	0.77	I	0.68
Standard	I	0.74	I	0.64	A	0.57	I	0.58	I	0.53

I-Inactive; A-Active

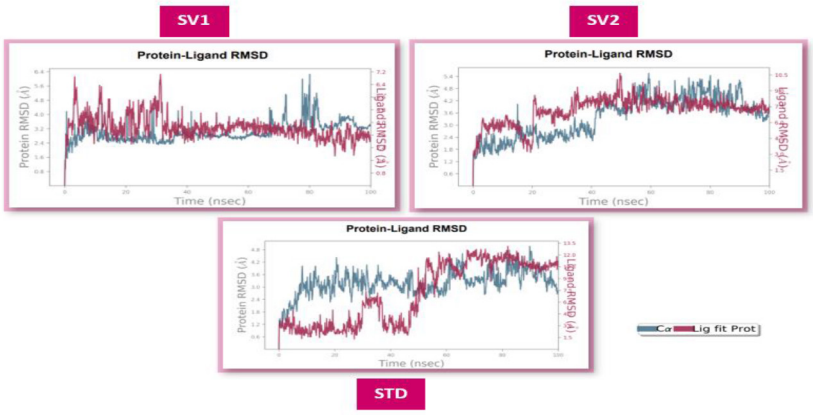


Figure 5. Protein ligand RMSD of the top two compounds and the standard (Talmapimod).

suggest that the designed compounds hold potential as safe drug candidates with lower risk for liver, genetic, immune, and cellular toxicity.

3.8 Molecular Dynamics

The molecular dynamics simulation of the Top 2 compounds SV1 and SV2 along with the standard Talmapimod in complex with the target MAPK p38α over a 100ns reveals the RMSD of protein-ligand complex, RMSF of residues, protein-ligand contacts and ligand properties to assess the binding stability of the ligand with the target.

3.8.1 Protein Ligand RMSD

The protein RMSD of the compound SV1 initially started at 1.5 Å, increased to 2.6-3.2 Å within the first 15 ns, and then dropped to 1.8 Å by 20 ns, indicating early conformational adjustments. Subsequently, the RMSD increased again to 3.6 Å and fluctuated between3.6-4.8 Å until 60 ns, before stabilizing in the range of 3.2-4.2 Å for the remaining time of the simulation, suggesting moderate but stable structural fluctuations. The ligand RMSD started at 3.0 Å and gradually increased to 6.0 Å by 40 ns, then remained relatively stable between 6.5-9.5 Å up to 100 ns, reflecting ligand adaptability within the binding site.

For compound SV2, the protein RMSD started at approximately 1.6 Å and fluctuated between 2.6-4.2 Å during the first 30 ns. It then decreased to around 2.6 Å and remained stable until 65 ns. Afterward, the RMSD increased again, ranging from 3.2-4.8 Å with occasional sharp fluctuations up to 80 ns, before

stabilizing between 3.2–3.5 Å for the remainder of the 100 ns simulation. The ligand RMSD began at 2.0 Å, fluctuated between 2.4-5.0 Å for the first 30 ns, then stabilized within 3.0-4.0 Å until 70 ns, and finally decreased to 2.4-3.5 Å by the end of the run.

For the standard compound, the protein RMSD began at 1.2 Å and increased steadily to 3.0 Å by 10 ns, followed by fluctuations between 2.4-3.8 Å until 45 ns. It then stabilized between 2.6-3.2 Å until 60 ns, increased slightly to 3.0-4.2 Å until 90 ns, and dropped back to 3.0 Å by 100 ns. The ligand RMSD started at 3.0 Å, remained between 1.5-3.2 Å until 30 ns, then increased to 4.5-6.5 Å by 40 ns, dropped again to 1.5-3.2 Å until 50 ns, and subsequently rose sharply to 12.0 Å by 60 ns. It then remained high, fluctuating between 9.0-12.0 Å until the end of the simulation, suggesting significant conformational movement or possible partial dissociation from the binding site. Figure 5 illustrates the protein ligand RMSD of SV1, SV2 and standard.

3.8.2 Protein Ligand RMSF

The SV1 compound exhibited good structural stability, as evidenced by residue fluctuations (RMSF) that remained mostly below 3.0 Å throughout the simulation. The ligand RMSF staying below 8.0 Å further supports the notion of a reasonably stable binding conformation, despite some dynamic flexibility.

The SV2 compound demonstrated good structural stability, as indicated by protein RMSF values mostly below 3.0 Å. The ligand RMSF remained below 2.0 Å supporting a stable binding conformation with minor dynamic fluctuations.

The standard compound maintained overall structural stability, as reflected by protein RMSF values staying mostly below 3.0 Å. The ligand RMSF stayed below 10.0 Å, supports the presence of a stable binding conformation, with minimal dynamic deviation. Figure 6 displays the protein ligand RMSF of SV1, SV2 and standard.

3.8.3 Protein Ligand Contacts

Protein-ligand interactions of compound SV1 formed hydrogen bonds along with water bridges with key residues such as Val 30, Asp 168, Ser 32, and Ser 154, with respective interaction fractions of 1.0, 1.1, 0.6, and 0.4 Å, suggesting stable and significant binding. A hydrophobic interaction with Ala51 was observed, with an interaction fraction of 0.2, further stabilizing the ligand within the active site.

For compound SV2, the protein-ligand interaction analysis revealed the formation of hydrogen bonds and water bridge interactions with key residues Lys53, Asp168, Glu71, and Gly33, each showing notable interaction fractions 1.2 - 0.6 Å that indicate strong and persistent contacts contributing to ligand stabilization.

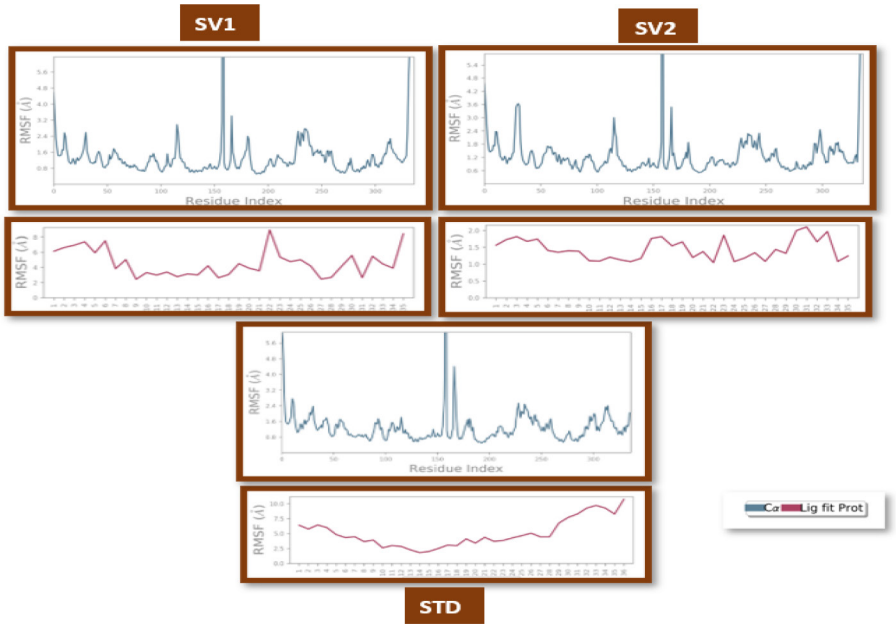


Figure 6. Protein ligand RMSF of the top two compounds and the standard (Talmapimod).

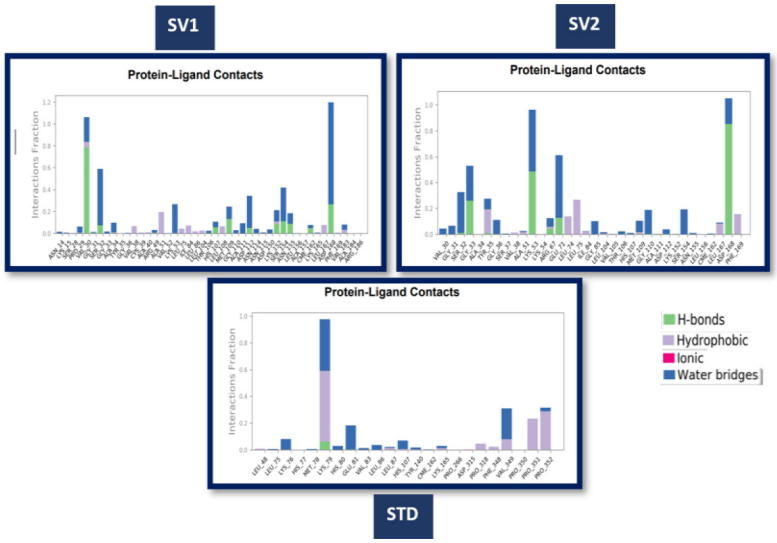


Figure 7. Protein ligand contact of the top two compounds and the standard (Talmapimod).

Additionally, moderate hydrophobic interactions were observed with residues Tyr35, Leu75, Leu74, and Phe169, with interaction fractions in the range of 0.2-0.3 Å, further supporting the stable positioning of the ligand within the binding pocket.

For the standard compound, the interaction profile showed hydrogen bonding, hydrophobic contacts, and water bridge interactions with Lys79, having an interaction fraction of 1.0 Å, signifying a strong stabilizing contact within the active site. Hydrophobic interactions were also formed with Pro351 and Pro352, with fraction values of 0.2 and 0.3, respectively. In addition, minor water bridge contacts were identified with Val349, contributing to the overall binding stability of the standard compound. Figure 7 depicts the protein ligand contacts of SV1, SV2 and standard.

3.8.4 Ligand Properties

For SV1, the ligand exhibited the radius of Gyration (rGyr) of the ligand remained within 4.8-5.6 Å for the first 40 ns and stabilized around 5.2 Å, indicating compact structural integrity. The ligand exhibited transient intramolecular hydrogen bonding, ranging from 0-2 bonds, suggesting occasional internal stabilization. The Molecular Surface Area (MolSA) remained stable between 445-460 Å², while the Solvent-Accessible Surface Area (SASA) increased from 160 Å² at the start to 250-400 Å² by 70 ns, eventually stabilizing between 300-350 Å² by the end of the simulation. The Polar Surface Area (PSA) ranged between 280-300 Å² until 30 ns, dropped to 260 Å² by 40 ns, and then maintained between 260-300 Å² throughout the rest of the simulation.

For SV2, the ligand maintained a radius of Gyration (rGyr) predominantly within 4.8-5.2 Å throughout the 100 ns simulation, indicating a persistently compact conformation. The number of intramolecular Hydrogen Bonds (intraHB) ranged between 0 and 1, suggesting occasional internal stabilization. The Molecular Surface Area (MolSA) remained stable within 420-435 Å², reflecting structural consistency. The solvent-accessible surface area (SASA) began above 200 Å², gradually decreased to 160-240 Å² by 30 ns, dropped further to about 80 Å² at 55 ns, and then stabilized between 80-160 Å² for the remainder of the simulation. The Polar Surface Area (PSA) was in the range of 260-300 Å² until 30 ns, after which it fluctuated between 160-300 Å² until 100 ns.

For the standard compound, the ligand showed a stable rGyr of 4.8-5.2 Å during the first 60 ns, which then slightly decreased to 4.4-5.2 Å until 85 ns and further to 4.4-4.8 Å by the end of the simulation. The MolSA remained consistent between 450-465 Å² until 45 ns, then slightly varied within 435-460 Å² until 100 ns. The SASA started at around 300 Å² and remained steady until 50 ns, after which it increased to approximately 600 Å², then decreased and stabilized between 300-450 Å², indicating periods of increased solvent exposure. The PSA remained relatively constant, fluctuating between 75-90 Å² throughout the simulation. Figure 8 represents the ligand properties of SV1, SV2 and standard.

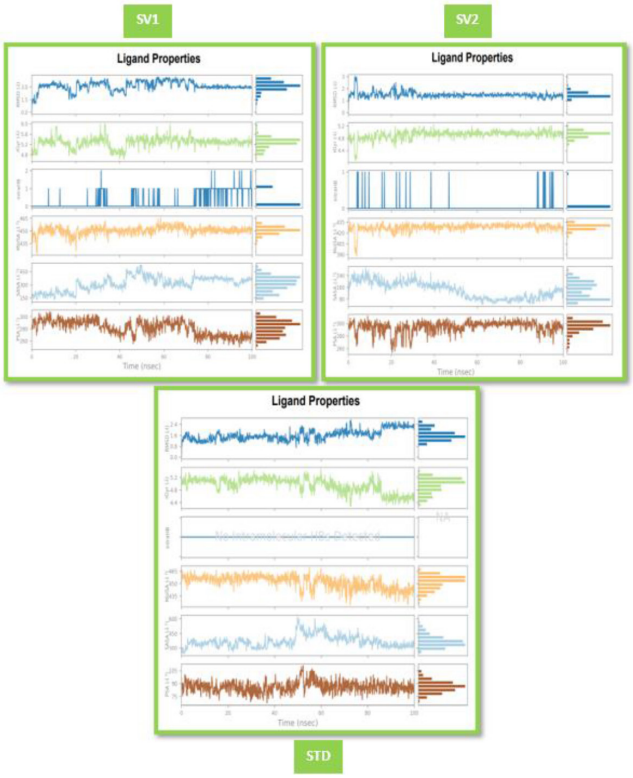


Figure 8. Ligand properties contact of the top two compounds and the standard (Talmapimod).

4. Conclusion

The present study demonstrated the identification of novel inhibitors targeting p38α MAPK, an important modulatory of inflammatory pathways implicated in asthma. A ligand-based pharmacophore model, constructed using MOE 2022, effectively incorporated crucial features essential for p38α MAPK inhibition. The model's reliability was validated through the DUDe platform, ensuring high selectivity in distinguishing active compounds from decoys. Virtual screening of natural compounds from the ZINC database yielded 365 potential hits, of which ten lead candidates (SV1-SV10) displayed favourable binding profiles in molecular docking studies. These compounds showed strong affinity and stable interactions with the active site residues of p38α MAPK. ADMET profiling confirmed drug-likeness, favourable pharmacokinetic properties, and non-toxic, non-carcinogenic behaviour for the top candidates. Among these, SV1 (ZINC38143592) and SV2 (ZINC04200785) emerged as the most promising, exhibiting optimal physicochemical properties and compliance with Lipinski's rule of five. Both molecules maintained stable hydrogen bonding with Asp168 and consistent binding throughout 100-nanosecond MD simulations, reflected by 3.2-4.0 Å for protein RMSD values. The ligand RMSD of SV2 compound was slightly higher than SV1 which indicates it adaptability in the active site. The ligand properties of both the compounds were compact with Rg 4.8-5.2 Å. Overall, SV1 and SV2 demonstrated strong inhibitory potential against p38α MAPK, indicating their suitability as therapeutic leads. These results demonstrated strong and stable interactions between selected natural compounds and the catalytic residues of MAPK p38α (Lys53, Thr106, and Asp168). Since p38α is a key regulator of cytokine production (TNF-α, IL-6, IL-1β) and airway inflammation, inhibition at the catalytic residues can suppress the phosphorylation responsible for NF-κB and AP-1 activation. Thus, the predicted binding interactions directly correlate with the down regulation of inflammatory mediators implicated in asthma pathophysiology. Therefore, it is evident that these natural compounds appear to be viable candidates for managing pulmonary inflammatory disorders.

5. Acknowledgements

We thank the Management of SRM College of Pharmacy and SRM Institute of Science and Technology for their constant support and encouragement. We also thank D. E. Shaw Research group for providing the academically free license for the Dynamics Desmond Suite of Schrodinger software.

6. Author Contribution

Varshini A. and Sanjana R. contributed to data collection, pharmacophore modelling, and virtual screening analyses. Bhuvaneswari Sivaraman guided computational studies, and contributed to data interpretation and manuscript preparation. Chagaleti Bharath Kumar supervised the project, validated computational results, and reviewed and revised the manuscript. All authors have read and agreed to the published version of the manuscript.

7. References

1. Venkatesan P. 2025 GINA report for asthma. Lancet Respir Med. 2025. PMID: 40582369. https://doi.org/10.1016/S2213-2600(25)00242-5

2. Bradding P. Asthma: Eosinophil disease, mast cell disease, or both?. Allergy Asthma Clin Immunol. 2008; 4(2):84. https://doi.org/10.1186/1710-1492-4-2-84
3. Jahan J, Barik S, Chagaleti BK, Kathiravan MK, Deivasigamani P. The synthetic approach of benzimidazole derivatives as anti-inflammatory agents. J med Pharm Allied Sci. 2023; 12(5). https://doi.org/10.55522/jmpas.v12i5.4826
4. Nakagome K, Nagata M. The possible roles of IL-4/IL-13 in the development of eosinophil-predominant severe asthma. Biomolecules. 2024; 14(5):546. https://doi.org/10.3390/biom14050546
5. Athari SS. Targeting cell signaling in allergic asthma. STTT. 2019; 4(1):45. https://doi.org/10.1038/s41392-019-0079-0
6. Pelaia C, Vatrella A, Gallelli L, Lombardo N, Sciacqua A, Savino R, Pelaia G. Role of p38 mitogen-activated protein kinase in asthma and COPD: Pathogenic aspects and potential targeted therapies. Drug Des Devel Ther. 2021; 15:1275-1284. https://doi.org/10.2147/dddt.s300988
7. Kim A, Lee CS. Apigenin reduces the Toll-like receptor-4-dependent activation of NF-κB by suppressing the Akt, mTOR, JNK, and p38-MAPK. Naunyn Schmiedebergs Arch Pharmacol. 2018; 391(3):271-283. https://doi.org/10.1007/s00210-017-1454-4
8. Athari SS. Targeting cell signaling in allergic asthma. STTT. 2019; 4(1):45. https://doi.org/10.1038/s41392-019-0079-0
9. Pascoe S, Costa M, Konczalik JM, McKie E, Yang S, Scherbovsky PS. Biological effects of p38 MAPK inhibitor losmapimod does not translate to clinical benefits in COPD. Respir Med. 2017; 130:20-26. https://doi.org/10.1016/j.rmed.2017.07.002
10. Jain KS, Bariwal JB, Kathiravan MK, Raskar VK, Wankhede GS, Londhe NA, Dighe SN. An efficient and rapid synthesis of 2-amino-4-arylthiazoles employing microwave irradiation in water. Green Sustain Chem. 2011; 1(2):35-38. https://doi.org/10.4236/gsc.2011.12007
11. Nayak SRPR, Haridevamuthu B, Murugan R, Dhivya LS, Venkatesan S, Almutairi MH, Almutairi BO, Kathiravan MK, Namasivayam SK, Arockiaraj J. Furan-based chalcone protects β-cell damage and improves glucose uptake in alloxan-induced zebrafish diabetic model *via* influencing Peroxisome Proliferator-Activated Receptor agonists (PPAR-γ) signaling. Process Biochem. 2024; 142:149-161. https://doi.org/10.1016/j.procbio.2024.04.012
12. Yang F, Zhao LJ, Xu Q, Zhao J. The journey of p38 MAP kinase inhibitors: From bench to bedside in treating inflammatory diseases. Eur J Med Chem. 2024; 280:116950. https://doi.org/10.1016/j.ejmech.2024.116950
13. Mouli HC, Vinod A, Kumari S, Tiwari AK, Kathiravan MK, Ravichandiran V, Peraman R. Deuterated driven new chemical entities: An optimistic way to improve therapeutic efficacy. Bioorg Chem. 2023; 135:106490. https://doi.org/10.1016/j.bioorg.2023.106490
14. Velmurugan BA, Sivaraman B, Natarajan R, Nagarajan N. Molecular docking studies on phytoconstituents of *Kabasura kudineer*-a *siddha* formulation on corona protease enzyme. Asian J Green Chem. 2022; 6(1):48-67. https://doi.org/10.22034/ajgc.2022.1.5
15. Mantharachalam D, Chagaleti BK, Anjana GV, Shanthakumar B. Exploring natural compound libraries for breast cancer targets: An *in silico* study. JNR. 2025; 25(3):639-656. https://doi.org/10.18311/jnr/2025/45930
16. Jayawardena TU, Sanjeewa KKA, Lee HG, Nagahawatta DP, Yang HW, Kang MC, Jeon YJ. Particulate matter-induced inflammation/oxidative stress in macrophages: Fucosterol from *Padina boryana* as a potent protector, activated *via* NF-κB/MAPK pathways and Nrf2/HO-1 involvement. Mar Drugs. 2020; 18(12):628. PMID: 33317054. PMCID: PMC7763233. https://doi.org/10.3390/md18120628
17. Yu JS, Kim AK. Wogonin induces apoptosis by activation of ERK and p38 MAPKs signaling pathways and generation of reactive oxygen species in human breast cancer cells. Mol Cells. 2011; 31(4):327-335. PMID: 21448585. PMCID: PMC3933962. https://doi.org/10.1007/s10059-011-0041-7
18. Epstein J, Docena G, MacDonald TT, Sanderson IR. Curcumin suppresses p38 mitogen-activated protein kinase activation, reduces IL-1β and matrix metalloproteinase-3 and enhances IL-10 in the mucosa of children and adults with inflammatory bowel disease. Br J Nutr. 2010; 103(6):824-832. PMID: 19878610. https://doi.org/10.1017/S0007114509992510
19. Pan W, Yu H, Huang S, Zhu P. Resveratrol protects against TNF-α-induced injury in human umbilical endothelial cells through promoting sirtuin-1-induced repression of NF-KB and p38 MAPK. Plos One. 2016; 11(1): e0147034. PMID: 26799794. PMCID: PMC4723256. https://doi.org/10.1371/journal.pone.0147034
20. Irrou E, Elmachkouri YA, Haddad SE, Chagaleti BK, Mague JT, MK K, Alotaibi SA, Gomha SM, Oubella A, Hassan O, Sebbar NK. Synthesis of novel N4-substituted and C2-disubstituted 1, 4-benzothiazine-1, 1-dioxide derivatives: Integrative computational strategies for breast cancer therapy. J Mol Struct. 2025; 1338:142310. https://doi.org/10.1016/j.molstruc.2025.142310
21. Usha T, Shanmugarajan D, Goyal AK, Kumar CS, Middha SK. Recent updates on computer-aided drug discovery: Time for a paradigm shift. Curr Top Med Chem. 2017; 17(30):3296-3307. PMID: 29295698. https://doi.org/10.2174/1568026618666180101163651
22. Chitre TS, Kathiravan MK, Bothara KG, Bhandari SV, Jalnapurkar RR. Pharmacophore optimization and design of competitive inhibitors of thymidine monophosphate kinase through molecular modeling studies. Chem Biol Drug Des. 2011; 78(5):826-834. PMID: 21801308. https://doi.org/10.1111/j.1747-0285.2011.01200.x
23. Pua LJW, Mai CW, Chung FF, Khoo ASB, Leong CO, Lim WM, Hii LW. Functional roles of JNK and p38 MAPK signaling in nasopharyngeal carcinoma. Int J Mol Sci. 2022;

23(3):1108. PMID: 35163030. PMCID: PMC8834850. https://doi.org/10.3390/ijms23031108

24. Chagaleti BK, Saravanan V, Kathiravan MK. Discovery of novel CDK2 inhibitors for cancer treatment: Integrating ligand-based pharmacophore modelling, molecular docking, DFT, ADMET, and molecular dynamics simulation studies. Beni Suef Univ J Basic Appl Sci. 2024; 13(118).
25. Zhang K, Fan Z, Wu Q, Liu J, Huang SY. Improved prediction of drug-protein interactions through physics-based few-shot learning. J Chem Inf Model. 2025. https://doi.org/10.1021/acs.jcim.5c00427.s001
26. Sivaraman B, Kathiravan MK. Targeting Aurora A kinase: Computational discovery of potent inhibitors through integrated pharmacophore and simulation approaches. Comput Biol Chem. 2025:108690. https://doi.org/10.1016/j.compbiolchem.2025.108690
27. Koes DR, Camacho CJ. ZINC Pharmer: Pharmacophore search of the ZINC database. Nucleic Acids Res. 2012; 40(W1):W409-W141. https://doi.org/10.1093/nar/gks378
28. Pranathi L, Kumar CB, Kumar AA, Devi KV. Design, synthesis, and docking studies of some new 5-(([1, 1'-Biphenyl]-4-yloxy) methyl)-2-(N-methylene) amino-1, 3, 4-thiadiazoles as anti-inflammatory agents. Indian J Heterocycl Chem. 2022; 32(4):461-468.
29. Gopinath P, Kathiravan MK. QSAR and docking studies on Triazole benzene sulfonamides with human Carbonic anhydrase IX inhibitory activity. Conference on Drug Design and Discovery Technologies. Royal Socirty of Chemistry. 2019; 33(12):e3189. https://doi.org/10.1039/9781839160783-00091
30. Mukhrish YE, Al-Humaidi JY, Chagaleti BK, Albedair LA, Gomha SM, Saravanan V, Kathiravan MK, Oubella A. Exploring the cyclization of Thiosemicarbazone to 1, 3, 4-Thiadiazole: Synthesis, characterization and *in-silico* study. J Mol Struct. 2024; 1322(Part 1):140385. https://doi.org/10.1016/j.molstruc.2024.140385
31. Babu NR, Sahoo BM, Radhika T, Malothu N. Synthesis, antitubercular evaluation, molecular docking study, and teratogenicity studies of novel triazolo quinazoline hybrids. Russ J Gen Chem. 2023; 93(10):2684-2693. https://doi.org/10.1134/s1070363223100237
32. Lipinski CA, Lombardo F, Dominy BW, Feeney PJ. Experimental and computational approaches to estimate solubility and permeability in drug discovery and development settings. Adv Drug Delivery Rev. 2012; 64:4-17. https://doi.org/10.1016/j.addr.2012.09.019
33. Daina A, Michielin O, Zoete V. SwissADME: A free web tool to evaluate pharmacokinetics, drug-likeness and medicinal chemistry friendliness of small molecules. Sci Rep. 2017; 7(42717). https://doi.org/10.1038/srep42717
34. Krishnu G, Paleti G, Chagaleti BK, Mueen A, Balakrishnan S. Design synthesis and evaluation of substituted benzimidazoles as potent polyketide synthase 13 inhibitors for tuberculosis. J Young Pharm. 2025; 17(1):149. https://doi.org/10.5530/jyp.20251380
35. Paleti G, Jena A, Krishnu G, Chagaleti BK, Bhimarao DP, Balakrishnan S. Innovative thiophene schiff bases: Synthesis and evaluation as antitubercular agents. Journal of Young Pharmacists. 2024; 16(4):735-744. https://doi.org/10.5530/jyp.2024.16.93
36. Jena A, Prakashraj C, Chagaleti BK, Kathiravan MK, Kumar BS. *In silico* design and synthesis of some new imidazole derivatives for tuberculosis. Indian J Heterocycl Chem. 2023; 33(1):43-49. https://doi.org/10.59467/ijhc.2023.33.43
37. Banerjee P, Eckert AO, Schrey AK, Preissner R. ProTox-II: A webserver for the prediction of toxicity of chemicals. Nucleic Acids Res. 2018; 46(W1): W257-W263. PMID: 29718510. PMCID: PMC6031011. https://doi.org/10.1093/nar/gky318
38. Laamari Y, Bimoussa A, Chagaleti BK, Saravanan V, Alotaibi SH, Alotaibi FM, Kathiravan MK, Oubella A, Itto MY, Auhmani A. Thymol-1, 2, 3-triazole derivatives: Network pharmacology, molecular simulations and synthesis targeting breast cancer. J Mol Struc. 2024; 1321(Part 4):140060. https://doi.org/10.1016/j.molstruc.2024.140060
39. Sadula A, Chagaleti BK, Enneiymy M, Peddaboina UR, Ankireddy A, Ajmi MFA, Oubella A. Multifaceted analysis of novel trisubstituted imidazole chromen derivatives: Design, synthesis, characterization, molecular docking, and antimicrobial evaluation. J Mol Struct. 2025; 1346:143185. https://doi.org/10.1016/j.molstruc.2025.143185
40. Chagaleti BK, Kumar BS, Rajagopal R, Alfarhan A, Arockiaraj J, Kumaradoss KM, Namasivayam SKR. Targeting cyclin-dependent kinase 2 CDK2: Insights from molecular docking and dynamics simulation-a systematic computational approach to discover novel cancer therapeutics. Comput Biol Chem. 2024; 112:108134. https://doi.org/10.1016/j.compbiolchem.2024.108134
41. Petrova T, Pesic J, Pardali K, Gaestel M, Arthur JSC. p38 MAPK signalling regulates cytokine production in IL-33 stimulated Type 2 innate lymphoid cells. Sci Rep. 2020; 10(3479). https://doi.org/10.1038/s41598-020-60089-0
42. Moulishankar, A, Sundarrajan, T. QSAR modeling, molecular docking, dynamic simulation and ADMET study of novel tetrahydronaphthalene derivatives as potent antitubercular agents. Beni Suef University J Basic and Appl Sci. 2023; 12(111). https://doi.org/10.1186/s43088-023-00451-z
43. Bellapukonda SM, Singothu S, Singampalli A, Bandela R, Kumar P, Yaddanapudi VM, Bhandari V, Nanduri S, Enneiymy M, AlAjm MF. Exploring spirocyclic isoquinoline-piperidine compounds in tuberculosis therapy: ADMET profiling, docking, DFT, MD simulations, and MMGBSA analysis. Comput Biol Chem. 2025; 118:108447. https://doi.org/10.1016/j.compbiolchem.2025.108447